Spin polarization and anomalous magnetic moment in a (2+1)-flavor Nambu–Jona-Lasinio model in a thermomagnetic background

Yi-Wei Qiu[1] and Sheng-Qin Feng[1,2,3,*]

[1]*College of Science, China Three Gorges University, Yichang 443002, China*
[2]*Key Laboratory of Quark and Lepton Physics (MOE) and Institute of Particle Physics, Central China Normal University, Wuhan 430079, China*
[3]*Center for Astronomy and Space Sciences, China Three Gorges University, Yichang 443002, China*

(Received 3 January 2023; accepted 23 March 2023; published 7 April 2023)

We investigate the magnetized QCD matter and chiral phase transition in a (2 + 1)-flavor Nambu–Jona-Lasinio (NJL) model at finite temperature and chemical potential by comparing the contributions from the tensor spin polarization (TSP) and anomalous magnetic moment (AMM) of quarks. For light u and d quarks, when TSP and AMM are not considered, the magnetized system is characterized by magnetic catalysis. The introduction of TSP will further enhance the magnetic catalytic characteristics. On the other hand, when AMM is introduced, the phase-transition temperature decreases with the magnetic field, which is the feature of inverse magnetic catalysis. The phase diagram of u and d quarks will change from the crossover phase transition to the first order phase transition with the increase of magnetic field and chemical potential when AMM is induced. The phase diagram will not change from the crossover phase transition to the first-order phase transition when TSP is induced. For the phase diagram of strange s quark, whether TSP or AMM is induced, the phase diagram will keep a crossover phase transition with the increase of magnetic field and chemical potential.

DOI: 10.1103/PhysRevD.107.076004

I. INTRODUCTION

Comprehending properties of QCD matter under a strong magnetic field is of essential importance to further investigate the evolution of the early Universe [1], noncentral heavy-ion collisions [2–5], neutron-star mergers [6,7], and the interior of magnetars [8,9]. The exploration of the QCD vacuum and strongly-interacting matter under external strong magnetic fields has attracted much attention (see reviews, e.g., Refs. [10–14]). Here we stress the study of the magnetic field of noncentral heavy-ion collisions, which comes from the laboratory simulations. The magnetic field reaches up to $\sqrt{eB} \sim 0.1$ GeV for RHIC and $\sqrt{eB} \sim 0.5$ GeV for LHC in noncentral heavy-ion collisions. This magnetic field is external since it is generated by the spectators, and though it has a very short lifetime (of the order of 1 fm/c). However, as shown in Refs. [15–18], the presence of the quark-gluon plasma (QGP) medium response effect, substantially delays the decay of these time-dependent magnetic fields. This is why in most cases, the effect of constant and uniform magnetic fields on quark matter is discussed in the literature. The magnetic field coincides with the production of the QGP and thus may have a fairly important effect on the properties of the phase transition such as the chiral magnetic effect (CME) [16,19–22], magnetic catalysis (MC) in the vacuum [23–25], inverse magnetic catalysis (IMC) around the chiral phase transition [26–29].

The magnetic field can lead to spin polarization, that is, the condensation of quark-antiquark $(\bar{q}q)$ pairs with spin parallel. Reference [30] shows that a tensor-type interaction $\sim(\bar{\psi}\Sigma^3\psi)^2 + (\bar{\psi}i\gamma^5\Sigma^3\psi)^2$ produces a spin polarization (SP) $\langle\bar{\psi}i\gamma^1\gamma^2\psi\rangle$, which is very similar to the anomalous magnetic moment (AMM) produced by quarks in a magnetic field. The tensor-polarization operator $\bar{\psi}\sigma^{\mu\nu}\psi$ can also be named as the spin-polarization operator, or the spin density since $\bar{\psi}\sigma^{12}\psi = \psi\gamma^0\Sigma^3\psi$. If the quark spinor ψ is projected into the subspin space $\psi = \psi_\uparrow + \psi_\downarrow$ corresponding to $\bar{\psi}\sigma^{12}\psi \sim \langle\bar{\psi}_\uparrow\psi_\uparrow\rangle - \langle\bar{\psi}_\downarrow\psi_\downarrow\rangle$, then this can be used to measure the difference between the spin-up quark pair and the spin-down quark pair.

We investigate the magnetized QCD matter in a (2 + 1)-flavor Nambu–Jona-Lasinio (NJL) model at finite temperature and chemical potential by comparing the contributions from the tensor spin polarization (TSP) and AMM of quarks. For a particle with charge e, mass m and

*Corresponding author.
fengsq@ctgu.edu.cn

spin $\vec{s}$, its corresponding magnetic moment (MM) is μ corresponding to the $\bar{q}q$ pair with antiparallel spin pairs, it has a net magnetic moment (MM), so the chiral condensation triggers a dynamic AMM. Under the action of the magnetic field, the net MM tends to be parallel to the magnetic field. For a SP with $\bar{q}q$ pair-parallel spin pairing, the MM of spin-aligned quarks and antiquarks cancel each other, and the spin-polarization pairing does not present a net MM. Therefore, compared with the chiral condensation with a nonzero net MM, the total MM of the system considering SP condensation will reduce. Therefore, systems with a spin polarization are expected to exhibit relative diamagnetism. At high temperatures, the pair of $\bar{q}q$ dissociates, and all charged quarks become a single small magnet, which are arranged in turn along the magnetic field. Therefore, QCD matter at high temperatures manifests paramagnetism.

The catalysis of chiral symmetry breaking induced by a magnetic field, namely the MC effect, can be easily understood from dimension reduction. On the other hand, IMC effect, the critical temperature of the chiral phase transition decreases with the increasing magnetic field, which is intuitively contradictory to the MC effect and is still a puzzle. There are many publications trying to explain IMC by considering running coupling constant generated by the magnetic field [31] and chiral imbalance caused by sphaleron transition or instanton anti-instanton pairing [32]. Some interesting and novel properties of magnetized QCD materials have recently been presented by lattice calculations, for example, magnetized materials exhibit paramagnetism (positive susceptibility) at high temperatures and diamagnetism (negative susceptibility) at low temperatures [33,34].

Recently, the effect of the AMM of quarks has drawn quite a lot of interest [35–41] in order to investigate the IMC effect. The dynamical chiral symmetry broken is known as one of the most important characteristics of QCD, which makes quarks achieve a dynamical mass of QCD. References [42,43] pointed out that quarks' AMM can also be dynamically produced like the dynamical quark mass. Therefore, once quarks achieve dynamical mass, they should also achieve dynamical AMM [42,44–46]. The coefficient κ of quarks' AMM in the magnetic field by the effective interaction $\frac{1}{2}q\kappa F_{\mu\nu}\bar{\psi}\sigma^{\mu\nu}\psi$ $(\sigma^{\mu\nu}=\frac{i}{2}[\gamma^{\mu},\gamma^{\nu}])$ is introduced, and the IMC effect at finite temperature is proposed by Ref. [47]. For QCD, both explicit and spontaneous chiral symmetry breaking are dedicated to the AMM of quarks, which is also called dynamical AMM [43].

In this paper, we investigate the magnetism of QCD matter and chiral phase transition with the contributions from the TSP and the AMM of quarks, respectively. This paper is organized as follows: We introduce the $(2+1)$-flavor NJL models by including the AMM and the TSP in Sec. II. In order to investigate the MC and IMC features by the AMM and TSP, the dependencies of dynamical mass, entropy, sound-velocity, and critical point on the magnetic field and temperature are studied in Sec. III. Finally, we make the summaries and conclusions in Sec. IV.

II. THE 2 + 1-FLAVORS NJL MODEL UNDER A MAGNETIC FIELD

The Lagrangian density of the $(2+1)$-flavor NJL model [48,49] in the presence of an external magnetic field is given as

$$\begin{aligned}\mathcal{L} &= \bar{\psi}(i\gamma^{\mu}D_{\mu}+\gamma^{0}\mu-m)\psi \\ &\quad + G_s\sum_{a=0}^{8}[(\bar{\psi}\lambda_a\psi)^2+(\bar{\psi}i\gamma^5\lambda_a\psi)^2] \\ &\quad - K[\det\bar{\psi}(1+\gamma_5)\psi+\det\bar{\psi}(1-\gamma_5)\psi], \end{aligned} \tag{1}$$

where the quark field ψ carries three flavors ($f=u,\ d,\ s$) and three colors ($c=r,\ g,\ b$), and $\lambda_a(a=1,\cdots N_f^2-1)$ represents the SU(3) Gell-Mann matrices in the three flavor space. Current quark mass m is considered as $m_u=m_d$ for isospin symmetry of light quarks, strange quark mass m_s is different from the other light quark (m_u and m_d) masses. The difference between the strange and nonstrange quark masses obviously breaks the SU(3) flavor symmetry. We assume that the quark chemical potentials of the strange and nonstrange quarks are the same, and take μ as the quark chemical potential. A covariant derivative with magnetic field is introduced as $D_u=\partial_\mu+\mathrm{i}\,QA_\mu^{\mathrm{ext}}$, and the charge matrix in flavor space is

$$Q=\mathrm{diag}(q_u,q_d,q_s)=\mathrm{diag}\left(\frac{2}{3},-\frac{1}{3},-\frac{1}{3}\right). \tag{2}$$

In general, if one chooses the gauge field $A_\mu^{\mathrm{ext}}=(0,0,Bx_1,0)$, the constant magnetic field should point at the x^3-direction. The K term of Eq. (1) is the Kobayashi-Maskawa–'t Hooft interaction term [49–51].

A. The introduction of a (2 + 1)-flavors NJL model with TSP

It is shown that [30,35] the breaking of the rotational symmetry by a uniform magnetic field induces a separation between longitudinal and transverse-fermion modes along the direction of the magnetic field. This separation gives rise to the effective splitting of the couplings in the one-gluon exchange interactions on which the NJL models are usually based. This splitting is therefore reported in the four-fermion couplings of a QCD-inspired NJL model in a magnetic field, and we can use the Fierz identities in a magnetic field [30,31,52] to propose the interactions of scalar and tensor of the $(2+1)$-flavor NJL Lagrangian,

$$\begin{aligned}\mathcal{L}_{\mathrm{TSP}} &= \bar{\psi}(i\gamma^{\mu}D_{\mu}+\gamma^{0}\mu-m)\psi \\ &+ G_s\sum_{a=0}^{8}[(\bar{\psi}\lambda_a\psi)^2+(\bar{\psi}i\gamma^5\lambda_a\psi)^2] \\ &+ G_t\sum_{a=0}^{8}\{(\bar{\psi}\Sigma_3\lambda_a\psi)^2+(\bar{\psi}\Sigma_3 i\gamma^5\lambda_a\psi)^2\} \\ &- K\{\det[\bar{\psi}(1+\gamma_5)\psi]+\det[\bar{\psi}(1-\gamma_5)\psi]\}. \end{aligned} \tag{3}$$

The coupling constant G_s in the scalar/pseudoscalar channel is closely related to the spontaneously chiral symmetry breaking, which produces a dynamical quark mass, and the tensor/pseudotensor channels term $G_t\sum_{a=0}^{8}[(\bar{\psi}_f^c\Sigma^3\lambda_a\psi_f^c)^2+(\bar{\psi}_f^c i\Sigma^3\gamma^5\lambda_a\psi_f^c)^2]$ is closely related to the spin-spin interaction, which causes spin-polarization condensation.

For the $(2+1)$-flavor NJL model, tensor-type interaction at the mean field level leads to the two types of spin polarization as

$$\begin{aligned} F_3 &= -2G_t\langle\bar{\psi}\Sigma^3\lambda_3\psi\rangle, \\ F_8 &= -2G_t\langle\bar{\psi}\Sigma^3\lambda_8\psi\rangle. \end{aligned} \tag{4}$$

In general, F_3 contains only u and d quark spin polarization condensates, on the other hand, F_8 is associated with the strange quark spin polarization condensate. The running coupling constants are divided into longitudinal ($g_{\parallel}$) and transverse ($g_{\perp}$) components due to the existence of the magnetic field. In our current study, the couplings of the above NJL interactions relevant to quark-gluon vertex coupling are expressed as $G_s=(g_{\parallel}^2+g_{\perp}^2)/\Lambda^2$ and $G_t=(g_{\parallel}^2-g_{\perp}^2)/\Lambda^2$. The distinguishing transverse and parallel Fierz identities automatically create a new channel of a four-fermion interaction term with second-order tensor structure in Lagrangian density during the transformation from splitting quark-gluon coupling to the scalar and pseudoscalar bilinear quantity [30]. G_s and G_t can be considered as the scalar and tensor channel interaction couplings, respectively.

The effective potential of using a standardized process is given

$$\begin{aligned}\Omega_{\mathrm{TSP}} &= G_s\sum_{f=u,d,s}\langle\bar{\psi}\psi\rangle_f^2+G_t\langle\bar{\psi}\lambda_3\Sigma^3\psi\rangle^2+G_t\langle\bar{\psi}\lambda_8\Sigma^3\psi\rangle^2 \\ &- \frac{N_c}{2\pi}\sum_{f=u,d,s}|q_fB|\sum_{l=0}^{\infty}\alpha_l\int_{-\infty}^{\infty}\frac{dp_z}{2\pi} \\ &\times\left\{\varepsilon_{f,l,\eta}+T\ln\left[1+\exp\left(\frac{-\varepsilon_{f,l,\eta}-\mu}{T}\right)\right]\right. \\ &\left.+T\ln\left[1+\exp\left(\frac{-\varepsilon_{f,l,\eta}+\mu}{T}\right)\right]\right\} \\ &+ 4K\langle\bar{\psi}\psi\rangle_u\langle\bar{\psi}\psi\rangle_d\langle\bar{\psi}\psi\rangle_s, \end{aligned} \tag{5}$$

where $l=0,1,2\ldots$ represents the quantum number of Landau level and $\eta=\pm1$ corresponds to the two kinds of the spin direction of quark-antiquark ($\bar{q}q$) pair. The contribution of nondegenerate particles due to spin difference at nonlowest Landau energy levels can be taken into account with the definition of this new operator $\alpha_l=\delta_{0,l}+\Delta(l)\sum_{\eta=\pm1}$, where $\Delta(l)$ is denoted by

$$\Delta(l)=\begin{cases}0 & l=0\\ 1 & l>0,\end{cases} \tag{6}$$

and the energy spectrum of the lowest Landau level (LLL) ($l=0$) and non-LLL ($l\neq0$) are given as

$$\begin{aligned}\varepsilon_{u,l=0}^2 &= p_z^2+\left(M_f+\left(F_3+\frac{F_8}{\sqrt{3}}\right)\right)^2, \\ \varepsilon_{u,l\neq0,\eta=\pm1}^2 &= p_z^2+\left(\sqrt{{M_f}^2+2|q_fB|l}+\eta\left(F_3+\frac{F_8}{\sqrt{3}}\right)\right)^2, \\ \varepsilon_{d,l=0}^2 &= p_z^2+\left(M_f+\left(F_3-\frac{F_8}{\sqrt{3}}\right)\right)^2, \\ \varepsilon_{d,l\neq0,\eta=\pm1}^2 &= p_z^2+\left(\sqrt{{M_f}^2+2|q_fB|l}+\eta\left(F_3-\frac{F_8}{\sqrt{3}}\right)\right)^2, \\ \varepsilon_{s,l=0}^2 &= p_z^2+\left(M_f+\left(\frac{2F_8}{\sqrt{3}}\right)\right)^2, \\ \varepsilon_{s,l\neq0,\eta=\pm1}^2 &= p_z^2+\left(\sqrt{{M_f}^2+2|q_fB|l}+\eta\left(\frac{2F_8}{\sqrt{3}}\right)\right)^2. \end{aligned} \tag{7}$$

Note that the breaking of energy-spectrum degeneracy caused by spin is known as the Zeeman effect. Therefore, the contributions of spin come not only from the ground state of the Landau levels, but also from the whole excited states of the Landau levels. The tensor-condensate parameter F_3 and F_8 are self-consistently satisfied the minimum of the thermodynamic potential, which are similar to dynamical quark mass M_f. At first, one can obtain three gap equations for M_f ($f=u,\,d,\,s$)

$$\frac{\partial\Omega_{\mathrm{TSP}}(M_f,F_3,F_8)}{\partial M_f}=0, \tag{8}$$

and the other two gap equations for F_3 and F_8 are given as

$$\begin{aligned}\frac{\partial\Omega_{\mathrm{TSP}}(M_f,F_3,F_8)}{\partial F_3}&=0, \\ \frac{\partial\Omega_{\mathrm{TSP}}(M_f,F_3,F_8)}{\partial F_8}&=0. \end{aligned} \tag{9}$$

To ensure that the thermodynamic potential in vacuum returns to zero, we define the normalized thermodynamic potential as the effective potential

$$\Omega_{\text{eff}}(T,\mu,eB) = \Omega(T,\mu,eB) - \Omega(0,0,eB). \quad (10)$$

Some of the relevant thermodynamical quantities can be evaluated by the effective potential. The quark number density is

$$\rho_f = \sum_{l,\eta} \frac{N_c|q_f eB|}{4\pi^2} \int_{-\infty}^{\infty} dp_z (n^+ - n^-), \quad (11)$$

where $n^{\pm} = 1/(\exp[(\varepsilon_{f,l,\eta} \mp \mu)/T] + 1)$ is quark (antiquark) number distribution. The entropy density $S_f = -\frac{\partial \Omega_{\text{eff}}}{\partial T}$ is given as

$$S_f = -\sum_{l,\eta} \frac{N_c|q_f eB|}{4\pi^2} \int_{-\infty}^{\infty} dp_z \Big[\ln(1-n^+) + \ln(1-n^-) - \frac{\varepsilon_{f,l,\eta}}{T}(n^+ + n^-) + \frac{\mu}{T}(n^+ - n^-)\Big]. \quad (12)$$

The energy density is given as

$$\varepsilon = T\frac{\partial P}{\partial T} + \mu\frac{\partial P}{\partial \mu} - P, \quad (13)$$

where P is pressure. The square of sound-speed is defined as

$$c_s^2 = \frac{\partial P}{\partial \varepsilon} = \left(\frac{\mu}{S_f}\frac{\partial \rho_f}{\partial T} + \frac{T}{S_f}\frac{\partial S_f}{\partial T}\right)^{-1}. \quad (14)$$

B. The introduction of the (2 + 1)-flavor NJL model with AMM

The effective Lagrangian density of the $(2+1)$-flavor with AMM [48,49] is given as

$$\mathcal{L}_{\text{AMM}} = \bar{\psi}\left(i\gamma^\mu D_\mu + \gamma^0\mu - m + \frac{1}{2}q_f\kappa\sigma^{\mu\nu}F_{\mu\nu}\right)\psi + G_s\sum_{a=0}^{8}[(\bar{\psi}\lambda_a\psi)^2 + (\bar{\psi}i\gamma^5\lambda_a\psi)^2] - K[\det\bar{\psi}(1+\gamma_5)\psi + \det\bar{\psi}(1-\gamma_5)\psi]. \quad (15)$$

The effective potential with AMM can be taken as

$$\Omega_{\text{AMM}} = G_s\sum_{f=u,d,s}\langle\bar{\psi}\psi\rangle_f^2 + 4K\langle\bar{\psi}\psi\rangle_u\langle\bar{\psi}\psi\rangle_d\langle\bar{\psi}\psi\rangle_s - \frac{N_c}{2\pi}\sum_{f=u,d,s}|q_f B|\sum_{l=0}^{\infty}\sum_{t=\pm1}\int_{-\infty}^{\infty}\frac{dp_z}{2\pi} \times \left\{E_{f,l,t} + T\ln\left[1+\exp\left(\frac{-E_{f,l,t}-\mu}{T}\right)\right] + T\ln\left[1+\exp\left(\frac{-E_{f,l,t}+\mu}{T}\right)\right]\right\}, \quad (16)$$

where

$$E_{f,l,t} = \sqrt{p_z^2 + ((M_f{}^2 + 2|q_f B|l)^{1/2} - t\kappa_f q_f eB)^2} \quad (17)$$

is the energy spectrum under different Landau energy levels, and $t = \pm 1$ corresponds to the two kinds of the spin direction of the $\bar{q}q$ pair. One can obtain three coupling gap equations for each order parameter as

$$\frac{\partial \Omega_{\text{AMM}}}{\partial M_f} = 0, \quad (18)$$

where $f = u,\ d,\ s$ are for the three different flavors. Thus we can obtain three dynamical quark masses of u, d, and s as

$$\begin{aligned} M_u &= m_u - 4G_s\langle\bar{\psi}\psi\rangle_u + 2K\langle\bar{\psi}\psi\rangle_d\langle\bar{\psi}\psi\rangle_s, \\ M_d &= m_d - 4G_s\langle\bar{\psi}\psi\rangle_d + 2K\langle\bar{\psi}\psi\rangle_u\langle\bar{\psi}\psi\rangle_s, \\ M_s &= m_s - 4G_s\langle\bar{\psi}\psi\rangle_s + 2K\langle\bar{\psi}\psi\rangle_u\langle\bar{\psi}\psi\rangle_d, \end{aligned} \quad (19)$$

where

$$\langle\bar{\psi}\psi\rangle_f = \frac{N_c G_s}{2\pi}\sum_{l=0}^{\infty}\alpha_l|q_f B|\int_{-\infty}^{+\infty}\frac{dp_z}{2\pi}\frac{M_f}{\varepsilon_{f,l,t}}\left(1 - \frac{s\kappa_f q_f B}{\hat{M}_{f,l,t}}\right) \times \left\{1 - \frac{1}{e^{\frac{\varepsilon_{f,l,t}+\mu}{T}}+1} - \frac{1}{e^{\frac{\varepsilon_{f,l,t}-\mu}{T}}+1}\right\} \quad (20)$$

corresponds to the chiral condensation of different quark flavors.

III. RESULTS AND DISCUSSIONS

To calibrate sets of parameters to applicable observables, parameters are chosen as $\Lambda = 631.4$ MeV, $m_u = m_d = 5.6$ MeV, $m_s = 135.7$ MeV, $\Lambda^2 G_s = 1.835$, and $K\Lambda^5 = 9.29$ [49,53]. The empirical values are given as $f_\pi = 93$ MeV, $m_\pi = 138$ MeV, $m_K = 495.7$ MeV, and $m_{\eta'} = 957.5$ MeV.

The tensor channel coupling constant G_t restricted by the magnetic fields ought to be zero in the case of the vanished magnetic field, and equals the value of G_s when $eB \to \infty$.

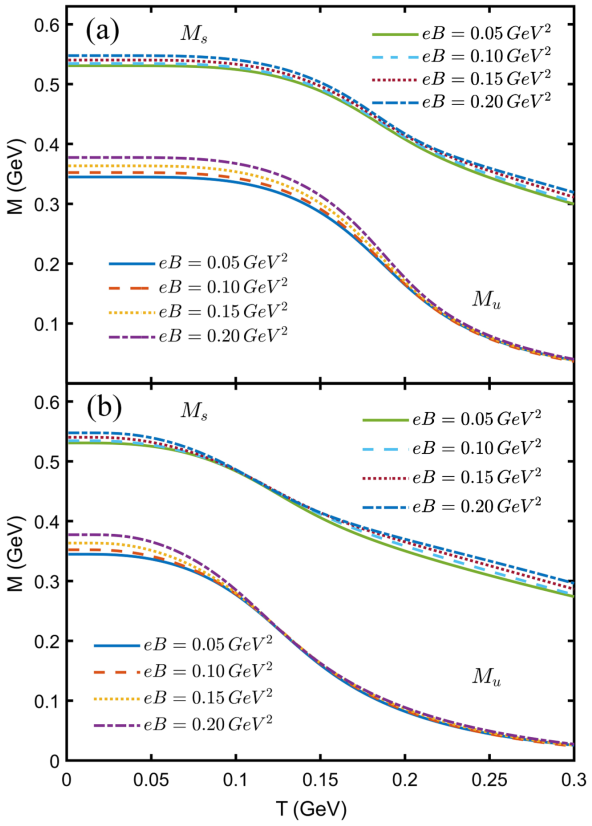

FIG. 1. The dependence of dynamical quark mass (M) on temperature (T) for four different magnetic fields ($eB = 0.05$, 0.10, 0.15, and 0.20 GeV^2) with no considering TSP and AMM. (a) is for $\mu = 0.0$ GeV and (b) is for $\mu = 0.25$ GeV.

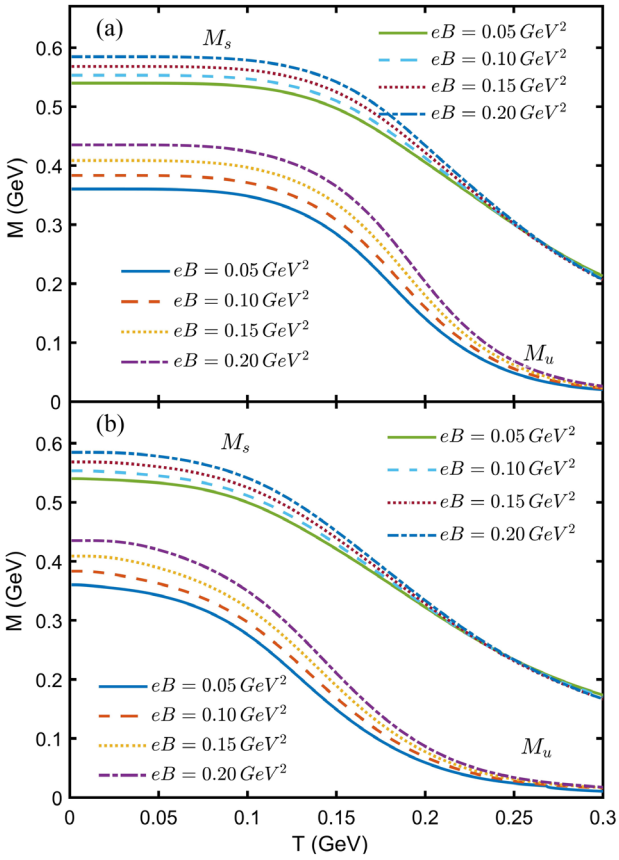

FIG. 2. The dependence of dynamical quark mass (M) on temperature (T) for four different magnetic fields ($eB = 0.05$, 0.10, 0.15, and 0.20 GeV^2) by considering TSP. (a) is for $\mu = 0.0$ GeV and (b) is for $\mu = 0.25$ GeV.

In the following study, the value of G_t is taken as $G_t = G_s/2$.

In order to investigate the effect of AMM on the phase transition, we make comparisons between the two AMM sets. The compatible results obtained in [54] we define it as AMM1 set as $\kappa_u = \kappa_d = 0.38, \kappa_s = 0.25$, while the defined AMM2 set chosen as $\kappa_u = 0.123, \kappa_d = 0.555, \kappa_s = 0.329$ fixed by [55].

Due to the NJL model being nonrenormalizable, the divergent vacuum terms merged in gap equation are regularized by using the magnetic-field-independent regularization scheme [56,57], which gets rid of the nonphysical part by separating the vacuum term from the integrals. The scheme dealing with the sums of all Landau levels within the integrals by means of the Hurwitz zeta function is presented. See the Appendix for detailed calculation results of F_3 and F_8 after regularization.

The dynamical mass or the quark condensate plays as an order parameter for the chiral-phase transition. Chiral restoration happens at high temperatures and/or high chemical potentials. In Figs. 1(a) and 1(b), the dynamical quark masses M of u, d, and s quarks without considering AMM and TSP are manifested as decreasing smooth functions of temperatures at $\mu = 0$ GeV and $\mu = 0.25$ GeV, which indicates a chiral crossover. The dynamical mass M is apparently enhanced by increasing the magnetic field. The magnetic field is shown at $eB = 0.05$, 0.1, 0.15, and 0.2 GeV^2 with $\mu = 0$ GeV and $\mu = 0.25$ GeV, respectively. Since we have considered nonvanishing current quark mass, the chiral symmetry is never restored fully. Since the dynamical mass is proportional to chiral condensate, it can be seen from Fig. 1 that the larger the magnetic field is, the larger the corresponding chiral condensation is. This phenomenon is manifested as magnetic catalysis [19,23,24,58], which accounts for the magnetic field has a strong tendency to enhance (or catalyze) spin-zero $\bar{q}q$ condensates.

By considering TSP of quarks, we investigate the temperature dependence of constituent quark mass in Figs. 2(a) and 2(b) for $eB = 0.05$, 0.10, 0.15 and 0.20 GeV^2, respectively. The dynamical mass M by considering TSP of quarks is manifested as a decreasing smooth function of temperatures for different magnetic fields and chemical potentials, which correspond to a chiral crossover. TSP is introduced by the anisotropic Fierz identity in NJL model, and moreover its essence is generated by symmetry broken caused by magnetic field B. The two tensor condensates $\langle\bar{\psi}\Sigma_3\lambda_3\psi\rangle$ and $\langle\bar{\psi}\Sigma_3\lambda_8\psi\rangle$

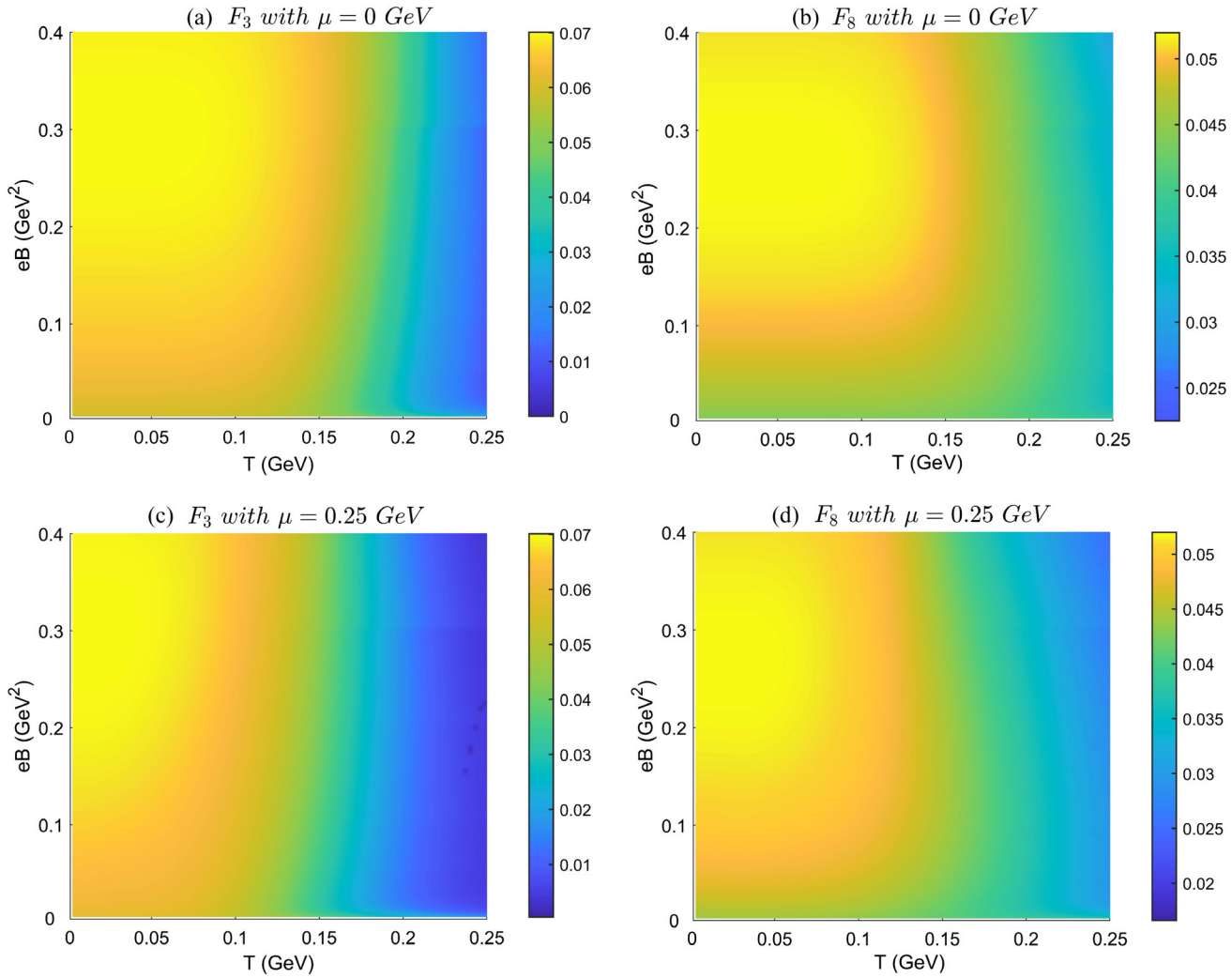

FIG. 3. (a),(b) shows the contour plots of the F_3 and F_8 distributions with zero chemical potential in the $T - eB$ plane, and (c),(d) shows similar plots of the F_3 and F_8 distributions but with nonzero chemical potential $\mu = 0.25$ GeV.

corresponding to TSP will provide a nonzero magnetic moment for the quasiparticle when the quark obtains the dynamical mass. The magnetic moment generated by the spin polarization under the action of the magnetic field will increase the dynamical mass of the quasiparticle, which leads to the MC effect. This MC characteristic of u and d quarks is more obvious in the high-temperature region.

In the $T - eB$ plane of Fig. 3, the corresponding temperature range is $0\ \text{GeV} \leq T \leq 0.3\ \text{GeV}$, and the magnetic field range is $0\ \text{GeV}^2 \leq eB \leq 0.5\ \text{GeV}^2$. Figures 3(a) and 3(b) displays the contour plots of the F_3 and F_8 distributions with a zero chemical potential in the $T - eB$ plane, and Figs. 3(c) and 3(d) shows similar plots of the F_3 and F_8 distributions but with nonzero chemical potential $\mu = 0.25$ GeV. The $(2 + 1)$-flavor spin polarization is different from that of two-flavor spin polarization because of an additional term $F_8 = -2G_t\langle\bar{\psi}\Sigma^3\lambda_8\psi\rangle$ associated with the λ_8 flavor generator.

Figure 3 shows that both F_3 and F_8 become stronger at low temperatures, especially with the increase of the magnetic field. F_3 is almost zero at high temperatures, and F_8 is very small but not zero at high temperatures. The polarizations become weak at high temperatures (chiral symmetry phase-restored area). It thus can be concluded that it is more difficult to be polarized in the hot QGP background.

Figure 4 displays the dependence of dynamical quark mass (M) on temperature (T) for four different magnetic fields ($eB = 0.05$, 0.10, 0.15, and 0.20 GeV^2) by considering the two AMM's sets. Figures 4(a) and 4(b) are for $\mu = 0$ GeV and $\mu = 0.25$ GeV with AMM1 set as $\kappa_u = \kappa_d = 0.38$, and $\kappa_s = 0.25$. Figures 4(c) and 4(d) is same as Figs. 4(a) and 4(b) but with AMM2 set as $\kappa_u = 0.123$, $\kappa_d = 0.555$, and $\kappa_s = 0.329$. Contrary to the behavior of the zero AMM in Fig. 1, the mass-decreasing behavior of u and d quarks in the chiral restoration is not a smooth slope but a sudden drop, which indicates the existence of a first-order transition. However, the smooth slope of the dynamical mass for the crossover can be still present in the weak field $eB = 0.05$ GeV^2 for the

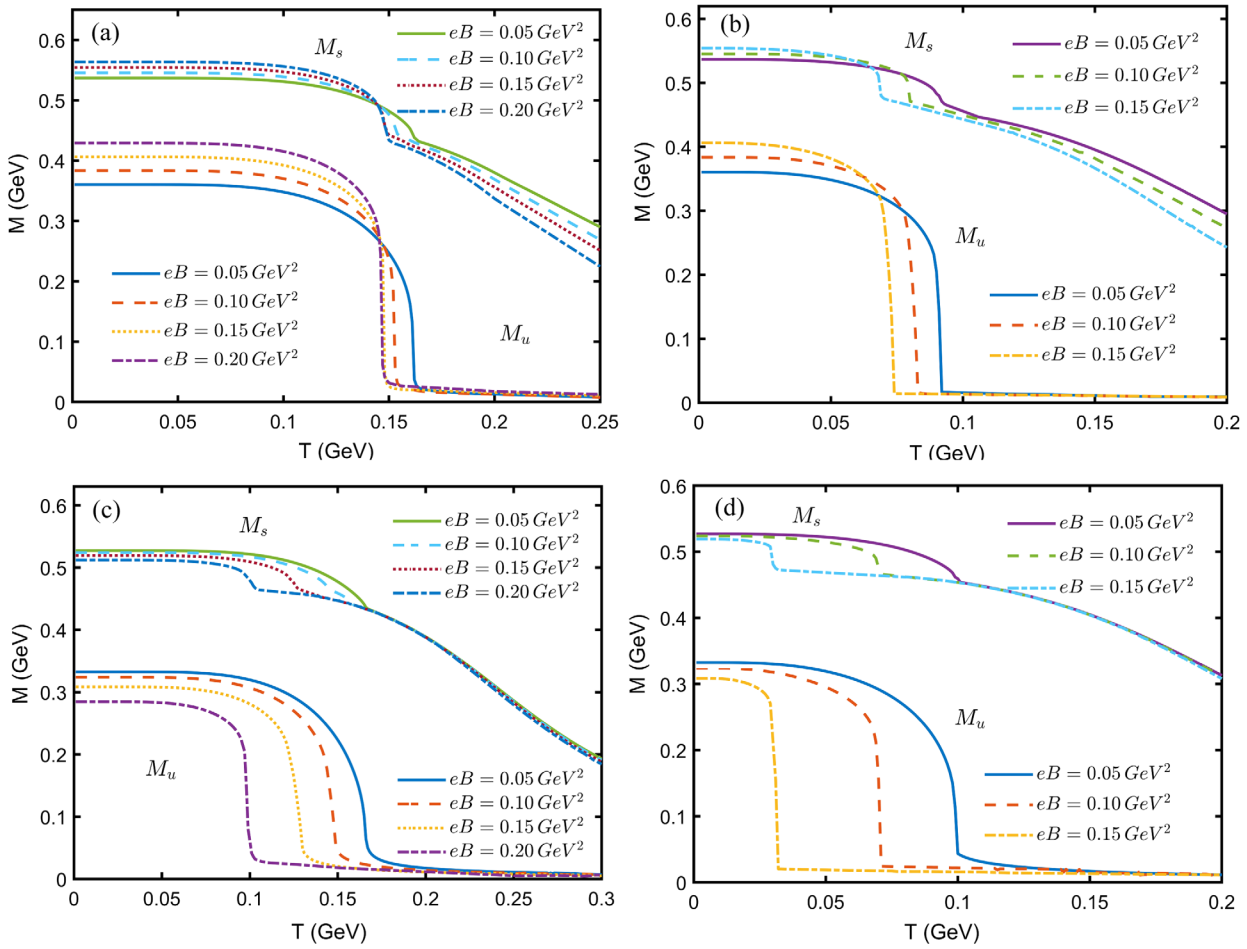

FIG. 4. The dynamical quark mass (M) as a function of temperature (T) for four different magnetic fields ($eB = 0.05$, 0.10, 0.15, and 0.20 GeV^2) by considering the different sets of AMM. (a) and (b) are for $\mu = 0$ and $\mu = 0.25$ GeV, respectively with AMM1 set as $\kappa_u = \kappa_d = 0.38$, $\kappa_s = 0.25$. (c),(d) is same as (a),(b) but for AMM2 set as $\kappa_u = 0.123$, $\kappa_d = 0.555$, $\kappa_s = 0.329$.

nonzero AMM. The mass-decreasing behavior of s quark in the chiral restoration is still a smooth slope, which suggests a chiral crossover for s quark. From Fig. 4, it is found that the dynamical quark mass of u and d quarks have the characteristics of inverse magnetic catalysis in the chiral restoration phase ($T \geq T_C$) by using the AMM sets.

The generation of dynamical quark mass from the dimensional reduction from $(3+1)$D to $(1+1)$D is

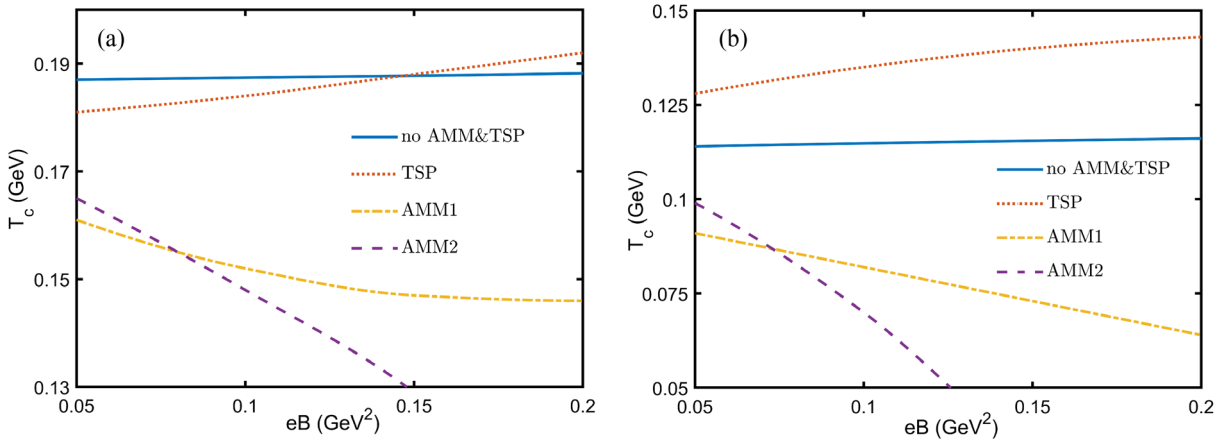

FIG. 5. The critical temperature of u and d quarks as a function of the magnetic field at $\mu = 0$ (a) and $= 0.25$ GeV (b).

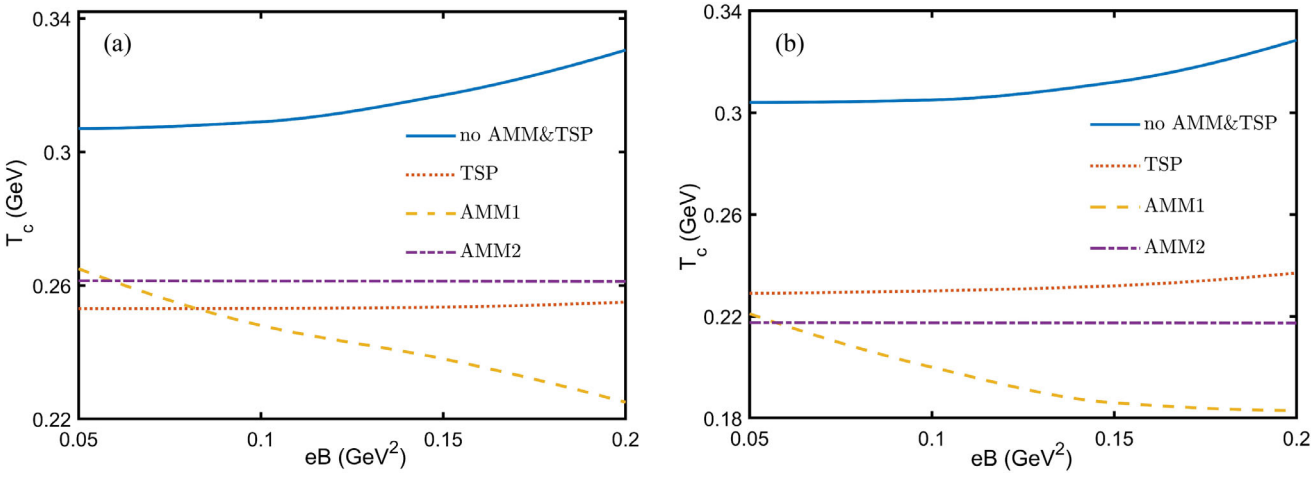

FIG. 6. The same as Fig. 5, but for the s-quark.

predominated by LLL at the low temperature region. That effect can be clearly reflected in AMM1 in Fig. 4. More particles will be excited from LLL to a higher Landau level (LL) with increasing temperatures. The contribution of particles on higher LL to the dynamical mass by considering the effect of the AMM will decrease with the increasing of magnetic field, leading to the inverse magnetic catalytic characteristics. If the role of the AMM item is enough to alter the nature of the medium in the $T = 0$ like the case of AMM2, the IMC effect characteristics of the AMM2 will be more significant.

In Fig. 5, the critical temperature is shown as a function of the magnetic field with the chemical potentials $\mu = 0$ GeV and 0.25 GeV, respectively. It is thus found that the critical temperature decreases with the magnetic field for the AMM1 and AMM2 sets, which indicates an inverse magnetic catalysis that qualitatively agrees with lattice result in [33]. On the contrary, with the TSP, T_C enhances as a function of the magnetic field, which is the extension of the magnetic catalysis effect from vacuum to finite temperature.

The critical temperature of the chiral phase transition of s quark as a function of eB is manifested in Fig. 6. Compared with light quarks of u and d, the phase-transition temperature T_C of s quark with TSP increases significantly with the increase of magnetic field, which corresponds to the characteristics of magnetic catalysis. The introduction of AMM sets corresponds to inverse magnetic-catalytic characteristics.

Figure 7 displays the dependencies of the entropy density of u, d, and s quarks on the temperature at zero chemical potential. It can be noted that the introduction of the AMM makes the crossover phase transition sharp. It is worth noting that the AMM in Fig. 7 corresponds to three different settings, which are AMM0, AMM1, and AMM2, respectively. AMM0 means that the AMM is not considered, that is, all κ values in Eq. (17) are set to zero. AMM1 and AMM2 sets have been mentioned above. When $eB = 0.05$ GeV^2, the magnetic field is not big enough to excite the effect on entropy. When $eB = 0.2$ GeV^2, some of the effects of the magnetic field on entropy for different AMM sets and TSP can be excited. It is found that the entropy shows a sharp change near the phase transition temperature after adding AMM sets, and this sharp change is more obvious with the magnetic field increases and chemical potential, showing a first-order phase characteristic. The

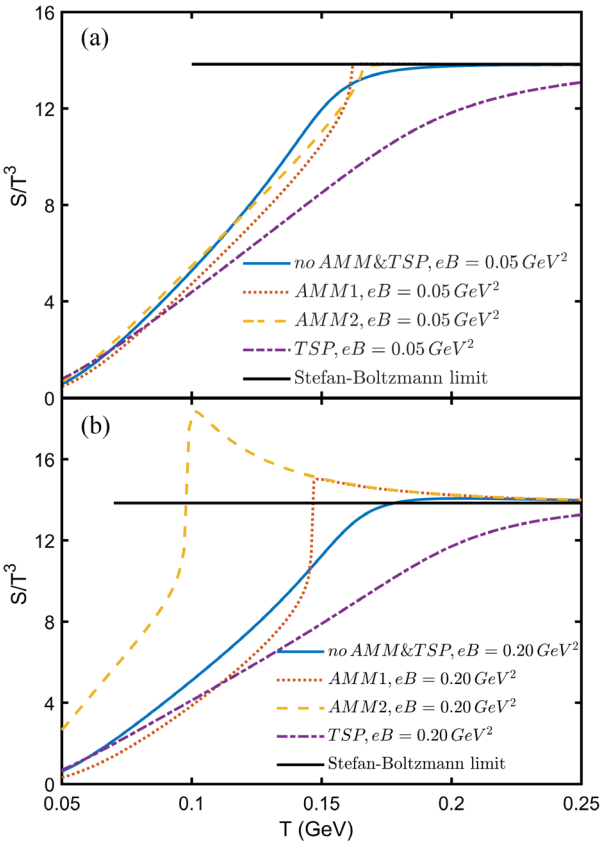

FIG. 7. The dependence of S/T^3 on temperature T at $\mu = 0$ GeV with different magnetic field. (a) is for $eB = 0.05$ GeV^2 and (b) is for $eB = 0.2$ GeV^2.

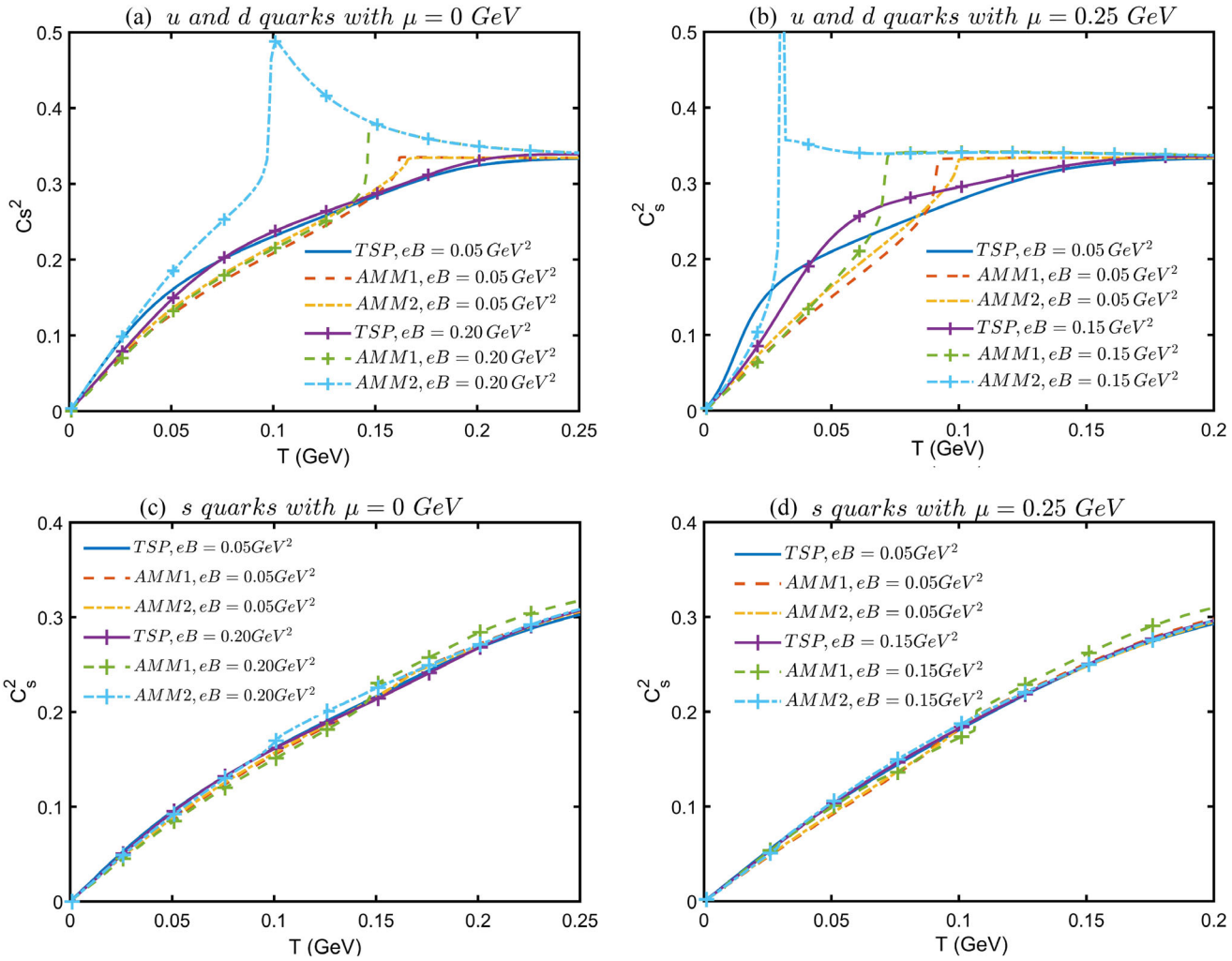

FIG. 8. The sound-velocity square C_s^2 of u and d with s quarks as a function of the temperature T with different chemical potential. (a),(b) is for u and d quarks with zero chemical potential $\mu = 0$ GeV and $\mu = 0.25$ GeV, and (c),(d) is for s quarks.

change of entropy with the temperature near the phase-transition temperature is relatively smooth after adding TSP, and it behaves like the crossover transition.

The dependence of square of sound-velocity c_s^2 on temperature T is manifested in Fig. 8. Figures 8(a) and 8(b) are for zero chemical potential $\mu = 0$ GeV and $\mu = 0.25$ GeV, respectively. In the region of crossover, the change of c_s^2 with temperature should be very smooth, while in the finite chemical potential region, the effect of AMM makes it incline to first-order transition. The bump rises rapidly because the dynamical quark mass has a discontinuous drop at this narrow region of temperature as shown in Fig. 4. Both sides of the narrow peak correspond to the hadron phase and quark-gluon plasma, and its highest point corresponds to the phase boundary. That leads our numerical result nearby the critical point of first-order transition to display nonphysical behavior even exceeding the Stefan-Boltzmann (S-B) limit. Similar result after the consideration of AMM of two flavor has been reported in [59].

Compared with u and d quarks, the square of sound-velocity of s quark with temperature is relatively smooth inflection after adding TSP and AMM sets. It is proposed that s quarks have always maintained obvious crossover characteristics. In the high-temperature region, the square of sound-velocity c_s^2 increases with temperature and obtains the saturation value $c_s^2 = 1/3$ to satisfy the relativistic requirement. This suggests that the equation of state in the chiral restoration phase at high temperatures is close to the Stefan-Boltzmann limit $\varepsilon = 3P$.

IV. SUMMARY AND CONCLUSIONS

In this work, we thoroughly study the effect from TSP and AMM on the vacuum, phase transition and thermal magnetized QCD in the $(2+1)$-flavor Nambu–Jona-Lasinio model with nonzero current quark masses at finite temperature and chemical potential. A unified physical mechanism to illustrate the novel consequences from recent

lattice QCD as magnetic catalysis and inverse magnetic catalysis effect is proposed in the paper.

In the TSP case, since the dynamical quark mass is increased by the spin condensate, which is generated by an extra tensor channel independently as well as enhanced by the magnetic field, the pseudocritical temperature is increased by a rising magnetic field. This is why the magnetic catalysis feature appears in the case of TSP. While in the AMM case, the AMM term $\frac{1}{2}q_f\kappa\delta^{\mu\nu}F_{\mu\nu}$ does not directly produce a new condensate to impact the dynamical mass. Instead, it changes the energy spectrum of all Landau levels. As the result, it has been found that the AMM term will reduce the dynamical mass once the temperature is high enough to excite particles to jump to higher Landau levels.

It is found that the square of sound-velocity shows a sudden rapid rise in inflection near the phase transition after adding AMM sets, and this rapid rise is more obvious with the magnetic field increases, showing an obviously first-order phase characteristic. On the other hand, after adding TSP, the change of square of sound-velocity with temperature near the phase transition is relatively smooth inflection, showing an obviously crossover transition characteristic. The result obtained by using the square of sound velocity is completely consistent with the result of entropy analysis.

The $(2+1)$-flavor spin polarization is different from that of two flavors because of an additional $F_8 = -2G_t\langle\bar{\psi}\Sigma^3\lambda_8\psi\rangle$ associated with the λ_8 flavor generator. The spin condensates affect the dynamical quark masses, chiral phase transition and quark dispersion relation. It is found that the polarizations become strong at low temperatures, and become weak at high temperatures. In other words, it is more difficult to be polarized in the hot QGP background, and easier to be polarized during the low-temperature region.

ACKNOWLEDGMENTS

This work was supported by the National Natural Science Foundation of China (Grants No. 11875178, No. 11475068, and No. 11747115).

APPENDIX

Following the regularization scheme to eliminate the divergent vacuum terms in the effective potential, the gap equation for F_3 and F_8 can be expressed as

$$\frac{\partial\Omega}{\partial F_3} = \mathrm{FVac}_u + \mathrm{FMag}_u + \mathrm{FMed}_u + \mathrm{FVac}_d + \mathrm{FMag}_d + \mathrm{FMed}_d - F_3 = 0, \tag{A1}$$

$$\frac{\partial\Omega}{\partial F_8} = \frac{1}{\sqrt{3}}(\mathrm{FVac}_u + \mathrm{FMag}_u + \mathrm{FMed}_u - \mathrm{FVac}_d - \mathrm{FMag}_d - \mathrm{FMed}_d) + 2(\mathrm{FVac}_s + \mathrm{FMag}_s + \mathrm{FMed}_s) - F_8 = 0, \tag{A2}$$

where the terms are

$$\mathrm{FVac}_f = \frac{N_c}{2\pi^2}(M_f + \mathrm{MX}_f)\left(\Lambda\sqrt{\Lambda^2 + {M_f}^2} - \frac{{M_f}^2}{2}\ln\left(\frac{(\Lambda + \sqrt{\Lambda^2 + {M_f}^2})^2}{{M_f}^2}\right)\right), \tag{A3}$$

$$\begin{aligned}\mathrm{FMag}_f = \frac{N_c|q_f eB|}{4\pi^2}\{&M_f \ln x_{f,-1} + \mathrm{MX}_f(\ln[\Gamma(x_{f,1})] + \ln[\Gamma(x_{f,-1})] + \ln 2\pi \\ &- (-x_{f,1} - x_{f,-1} + x_{f,-1}\ln x_{f,-1} + x_{f,1}\ln x_{f,1}))\},\end{aligned} \tag{A4}$$

$$\begin{aligned}\mathrm{FMed}_f = \frac{N_c|q_f eB|}{4\pi^2}\Bigg\{&\int_{-\infty}^{\infty} dp_z \frac{\mathrm{MX}_f + M_f}{E_{f,l=0}}\left(\frac{1}{1+\exp\left(\frac{E_{f,l=0}-\mu}{T}\right)} + \frac{1}{1+\exp\left(\frac{E_{f,l=0}+\mu}{T}\right)}\right) \\ &+ \sum_{l=1}^{\infty}\alpha_l\int_{-\infty}^{\infty} dp_z \frac{\mathrm{MX}_f + \eta M_f}{E_{f,l,\eta}}\left(\frac{1}{1+\exp\left(\frac{E_{f,l,\eta}-\mu}{T}\right)} + \frac{1}{1+\exp\left(\frac{E_{f,l,\eta}+\mu}{T}\right)}\right)\Bigg\},\end{aligned} \tag{A5}$$

where $x_{f,\eta}$ and MX_f are given as

$$x_{f,\eta} = \frac{1}{2|q_f eB|}({M_f}^2 + {\mathrm{MX}_f}^2 + 2\eta M_f \mathrm{MX}_f), \tag{A6}$$

$$\mathrm{MX}_u = \frac{F_3 + F_8}{\sqrt{3}},$$
$$\mathrm{MX}_d = \frac{F_3 - F_8}{\sqrt{3}},$$
$$\mathrm{MX}_s = \frac{2F_8}{\sqrt{3}}, \tag{A7}$$

where the η indicates the spin label ± 1.

[1] T. Vachaspati, Phys. Lett. B **265**, 258 (1991).
[2] V. Skokov, A. Y. Illarionov, and V. Toneev, Int. J. Mod. Phys. A **24**, 5925 (2009).
[3] W.-T. Deng and X.-G. Huang, Phys. Rev. C **85**, 044907 (2012).
[4] Y.-J. Mo, S.-Q. Feng, and Y.-F. Shi, Phys. Rev. C **88**, 024901 (2013).
[5] Y. Zhong, C.-B. Yang, X. Cai, and S.-Q. Feng, Adv. High Energy Phys. **2014**, 193039 (2014).
[6] K. Kiuchi, P. Cerdá-Durán, K. Kyutoku, Y. Sekiguchi, and M. Shibata, Phys. Rev. D **92**, 124034 (2015).
[7] L. Baiotti and L. Rezzolla, Rep. Prog. Phys. **80**, 096901 (2017).
[8] T. Tatsumi, AIP Conf. Proc. **847**, 171 (2006).
[9] R. C. Duncan and C. Thompson, Astrophys. J. Lett. **392**, L9 (1992).
[10] A. Bzdak, S. Esumi, V. Koch, J. Liao, M. Stephanov, and N. Xu, Phys. Rep. **853**, 1 (2020).
[11] D. E. Kharzeev, J. Liao, S. A. Voloshin, and G. Wang, Prog. Part. Nucl. Phys. **88**, 1 (2016).
[12] X.-G. Huang, Rep. Prog. Phys. **79**, 076302 (2016).
[13] J. O. Andersen, W. R. Naylor, and A. Tranberg, Rev. Mod. Phys. **88**, 025001 (2016).
[14] V. A. Miransky and I. A. Shovkovy, Phys. Rep. **576**, 1 (2015).
[15] U. Gursoy, D. Kharzeev, and K. Rajagopal, Phys. Rev. C **89**, 054905 (2014).
[16] D. She, S.-Q. Feng, Y. Zhong, and Z.-B. Yin, Eur. Phys. J. A **54**, 48 (2018).
[17] B.-X. Chen and S.-Q. Feng, Chin. Phys. C **44**, 024104 (2020).
[18] X. Chen, S.-Q. Feng, Y.-F. Shi, and Y. Zhong, Phys. Rev. D **97**, 066015 (2018).
[19] D. E. Kharzeev, L. D. McLerran, and H. J. Warringa, Nucl. Phys. **A803**, 227 (2008).
[20] K. Fukushima, D. E. Kharzeev, and H. J. Warringa, Phys. Rev. D **78**, 074033 (2008).
[21] Y. Guo, S. Shi, S. Feng, and J. Liao, Phys. Lett. B **798**, 134929 (2019).
[22] J. Deng and S.-Q. Feng, Phys. Rev. D **105**, 026015 (2022).
[23] V. P. Gusynin, V. A. Miransky, and I. A. Shovkovy, Nucl. Phys. **B563**, 361 (1999).
[24] V. P. Gusynin, V. A. Miransky, and I. A. Shovkovy, Nucl. Phys. **B462**, 249 (1996).
[25] S. P. Klevansky and R. H. Lemmer, Phys. Rev. D **39**, 3478 (1989).
[26] G. S. Bali, F. Bruckmann, G. Endrodi, F. Gruber, and A. Schaefer, J. High Energy Phys. 04 (2013) 130.
[27] G. S. Bali, F. Bruckmann, G. Endrodi, Z. Fodor, S. D. Katz, and A. Schafer, Phys. Rev. D **86**, 071502 (2012).
[28] G. S. Bali, F. Bruckmann, G. Endrodi, Z. Fodor, S. D. Katz, S. Krieg, A. Schafer, and K. K. Szabo, J. High Energy Phys. 02 (2012) 044.
[29] M. D'Elia, F. Manigrasso, F. Negro, and F. Sanfilippo, Phys. Rev. D **98**, 054509 (2018).
[30] E. J. Ferrer, V. de la Incera, I. Portillo, and M. Quiroz, Phys. Rev. D **89**, 085034 (2014).
[31] E. J. Ferrer, V. de la Incera, and X. J. Wen, Phys. Rev. D **91**, 054006 (2015).
[32] J. Chao, P. Chu, and M. Huang, Phys. Rev. D **88**, 054009 (2013).
[33] G. S. Bali, F. Bruckmann, M. Constantinou, M. Costa, G. Endrodi, S. D. Katz, H. Panagopoulos, and A. Schafer, Phys. Rev. D **86**, 094512 (2012).
[34] G. S. Bali, G. Endrődi, and S. Piemonte, J. High Energy Phys. 07 (2020) 183.
[35] S. Fayazbakhsh and N. Sadooghi, Phys. Rev. D **90**, 105030 (2014).
[36] E. J. Ferrer, V. de la Incera, D. Manreza Paret, A. Pérez Martínez, and A. Sanchez, Phys. Rev. D **91**, 085041 (2015).
[37] N. Chaudhuri, S. Ghosh, S. Sarkar, and P. Roy, Phys. Rev. D **99**, 116025 (2019).
[38] S. Ghosh, N. Chaudhuri, S. Sarkar, and P. Roy, Phys. Rev. D **101**, 096002 (2020).
[39] N. Chaudhuri, S. Ghosh, S. Sarkar, and P. Roy, Eur. Phys. J. A **56**, 213 (2020).
[40] S. Mao and D. H. Rischke, Phys. Lett. B **792**, 149 (2019).
[41] J. Mei and S. Mao, Phys. Rev. D **102**, 114035 (2020).
[42] E. J. Ferrer and V. de la Incera, Nucl. Phys. **B824**, 217 (2010).
[43] L. Chang, Y.-X. Liu, and C. D. Roberts, Phys. Rev. Lett. **106**, 072001 (2011).
[44] E. J. Ferrer and V. de la Incera, Phys. Rev. Lett. **102**, 050402 (2009).
[45] F. Preis, A. Rebhan, and A. Schmitt, J. High Energy Phys. 03 (2011) 033.

[46] P. J. A. Bicudo, J. E. F. T. Ribeiro, and R. Fernandes, Phys. Rev. C **59**, 1107 (1999).
[47] K. Xu, J. Chao, and M. Huang, Phys. Rev. D **103**, 076015 (2021).
[48] M. Buballa, Phys. Rep. **407**, 205 (2005).
[49] T. Hatsuda and T. Kunihiro, Phys. Rep. **247**, 221 (1994).
[50] U. Vogl and W. Weise, Prog. Part. Nucl. Phys. **27**, 195 (1991).
[51] P. Rehberg, S. P. Klevansky, and J. Hufner, Phys. Rev. C **53**, 410 (1996).
[52] F. Lin, K. Xu, and M. Huang, Phys. Rev. D **106**, 016005 (2022).
[53] H. Kohyama, D. Kimura, and T. Inagaki, Nucl. Phys. **B906**, 524 (2016).
[54] M. Mekhfi, Phys. Rev. D **72**, 114014 (2005).
[55] Y. Dothan, Physica (Amsterdam) **114A**, 216 (1982).
[56] D. P. Menezes, M. Benghi Pinto, S. S. Avancini, A. Perez Martinez, and C. Providencia, Phys. Rev. C **79**, 035807 (2009).
[57] R. M. Aguirre, Phys. Rev. D **102**, 096025 (2020).
[58] V. P. Gusynin, V. A. Miransky, and I. A. Shovkovy, Phys. Rev. Lett. **73**, 3499 (1994).
[59] X.-J. Wen, R. He, and J.-B. Liu, Phys. Rev. D **103**, 094020 (2021).